Numerical Study of Carrier Multiplication Pathways in Photoexcited Nanocrystal and Bulk Forms of PbSe

Kirill A. Velizhanin and Andrei Piryatinski*

Center for Nonlinear Studies (CNLS), Theoretical Division, Los Alamos National Laboratory, Los Alamos, New Mexico 87545, USA

(Received 19 October 2010; published 20 May 2011)

Employing the interband exciton scattering model, we perform a numerical study of the direct photogeneration and population relaxation processes contributing to carrier multiplication (CM) in nanocrystalline and bulk PbSe. We argue that in *both* cases the impact ionization is the main mechanism of CM. This explains the weak contribution of the direct photogeneration to the total quantum efficiency (QE). An investigation of the size scaling of QE in nanocrystals and a comparison to the bulk limit provide microscopic insight into the experimentally observed trends.

DOI: 10.1103/PhysRevLett.106.207401 PACS numbers: 78.67.Bf, 73.21.La, 78.47.−p, 78.67.Hc

Recent demand in new efficient photovoltaic devices has turned significant attention to the problem of carrier multiplication (CM) in semiconductor materials [1,2]. Early reported ultrafast spectroscopic studies of nanocrystals (NCs) [3–5] suggested that nanostructuring is a direct way to highly increase the CM quantum efficiency (QE), i.e., the number of excitons produced per absorbed photon. This was supported by the following arguments: An enhancement of the Coulomb interaction between carriers due to their spatial confinement should lead to more efficient biexciton production. Relaxation of the quasimomentum conservation constraint by breaking the translational symmetry should open additional pathways for CM while the intraband cooling is slowed down by the presence of the phonon bottleneck. More recent reports claim much lower QE or the absence of CM in NCs [6–9]. The controversy possibly arises from experimental inaccuracy [8], sample-to-sample variation in surface properties [10], and contribution from extraneous effects, e.g., photocharging [11,12]. Comparison to the bulk PbS and PbSe spectroscopic measurements shows that bulk QE exceeds validated QE in NCs if compared on the scale of absolute energy [13]. These issues call for the reassessment of the quantum confinement role in the CM dynamics [7].

From the theory point of view, multiexciton photogeneration [5,14], coherent multiexciton production [15,16], and incoherent impact ionization (II) [17–19] are currently under debate as primary mechanisms of CM. The *ab initio* calculations on small clusters ($\lesssim 1$ nm) demonstrated the role of strong Coulomb correlations in multiexciton photogeneration and emphasized the role of fast exciton-biexciton dephasing [20]. Atomistic calculations focused on small diameter ($\lesssim 3$ nm) NCs show that CM is dominated by II processes [19,21]. An extrapolation of these calculations to larger NCs and comparison to the bulk have been reported recently [22]. Effective mass models have been used to study direct photogeneration [23] and coherent CM dynamics in larger (4–6 nm) diameter NCs. Reported experimental studies consider even larger diameter ($\lesssim 10$ nm) NCs. However, no systematic investigation of all predicted CM pathways contributing to the ultrafast spectroscopic signal (i.e., photogeneration and population relaxation) in various size NCs and comparison to the bulk limit has been reported yet.

In this Letter, we report on such a study employing the interband exciton scattering model (IESM) [24] parametrized for PbSe materials. The IESM treats on equal footing the biexciton photogeneration during interaction with the pump pulse and subsequent population relaxation processes. This allows us to evaluate the contributions of all predicted pathways to the total QE. To clarify the quantum confinement effect on the key quantities determining QE, comparison with the bulk limit is reported on the absolute energy scale [7,22]. In general, performance of the photovoltaic devices can be characterized by variously defined power efficiency [12,22], in particular, using the photon energy scale normalized per NC or bulk band gap energy [25]. Since we focus on fundamental mechanisms of CM rather than applications, the latter unitless scale is not used below.

We consider an ensemble of NCs in which no more than one photon can be absorbed per NC leading to production of either exciton or biexciton state. Hence, QE can be defined as

$$\mathrm{QE} = (2N_{xx} + N_x)/(N_{xx} + N_x), \tag{1}$$

where N_x and N_{xx} are the ensemble nonequilibrium exciton and biexciton populations, respectively. For an ensemble of NCs, the bulk limit can be defined as the thermodynamic limit: $V \to \infty$, $V/v \to \infty$, and $v = \text{const}$. Here, V is a NC volume, v is the unit cell volume, and ratio V/v gives the number of unit cells. Since QE [Eq. (1)] is volume independent in the bulk limit, it is referred to as the intensive parameter. As a result, its scaling with NC size compared to the bulk limiting value provides a convenient measure of the quantum size effects. In general, the populations N_x and N_{xx} as well as density of states (DOS) and Coulomb

interactions (determining N_x and N_{xx}) are not intensive quantities. To make proper comparison with the bulk limit, below, we eliminate their volume scaling by multiplying them with powers of (v/V).

We start by defining the populations n_a^x and n_k^{xx} of ath exciton and kth biexciton states, respectively. Their time evolution during the interaction with the pump pulse (photogeneration) and subsequent population relaxation are numerically calculated using the weak Coulomb limit of IESM [24]. To account for the high DOS region in which CM dynamics occur, we recast n_a^x, and n_k^{xx} to the quasicontinuous frequency representation: $n_x(\omega) = \sum_{a\geq 1} n_a^x \delta(\omega - \omega_a^x)$ and $n_{xx}(\omega) = \sum_{k\geq 1} n_k^{xx}\delta(\omega - \omega_k^{xx})$. Accordingly, the intensive populations entering Eq. (1) become defined as $N_x = (v/V)\int_0^\infty d\omega n_x(\omega)$ and $N_{xx} = (v/V)\int_0^\infty d\omega n_{xx}(\omega)$.

In most ultrafast CM experiments, the pump duration exceeds typical dephasing time leading to the continuous wave (cw) excitation regime. Our simulations show that, in agreement with Ref. [16], high DOS leads to the suppression of the oscillating terms that contribute to n_a^x and n_k^{xx}. The IESM predicts interference of the photogeneration pathways contributing to n_k^{xx} [24]. However, the simulations show that due to high DOS, the sign-varying terms cancel out, fully eliminating the interference. Taking all of this into account, the cw photogenerated biexciton population can be represented as

$$N_{xx}(\omega_{pm}) = \frac{\mathcal{A}}{\hbar^2}\int d\omega' [V_{\text{eff}}^{x,xx}(\omega_{pm},\omega')]^2 \frac{\tilde{\rho}_x(\omega_{pm})\rho_{xx}(\omega')}{(\omega' - \omega_{pm})^2 + \gamma^2} + \frac{\mathcal{A}}{\hbar^2}\int d\omega' [V_{\text{eff}}^{x,xx}(\omega',\omega_{pm})]^2 \frac{\tilde{\rho}_x(\omega')\rho_{xx}(\omega_{pm})}{(\omega' - \omega_{pm})^2 + \gamma^2} + \frac{A}{\hbar^2}\int d\omega' [V_{\text{eff}}^{xx}(\omega')]^2 \frac{\tilde{\rho}_{xx}(\omega'\omega_{pm})}{\omega'^2}, \quad (2)$$

and the leading contribution to the exciton population as $N_x(\omega_{pm}) = \mathcal{A}\tilde{\rho}_x(\omega_{pm})$. Here, $\mathcal{A}$ is proportional to the pump fluence, ω_{pm} is the pump frequency, and γ is the dephasing rate of exciton-biexciton coherences. $\rho_x(\omega) = (v/V)^2\sum_a \delta(\omega - \omega_a^x)$ and $\rho_{xx}(\omega) = (v/V)^4\sum_k \delta(\omega - \omega_k^{xx})$ are intensive exciton and biexciton DOS, respectively. The associated optically allowed exciton DOS is $\tilde{\rho}_x(\omega) = (v/V)\sum_a |\mu_a^x|^2\delta(\omega - \omega_a^x)$ and joint biexciton DOS is $\tilde{\rho}_{xx}(\omega_1,\omega_2) = (v/V)^4\sum_{kl}|\mu_{kl}^{xx}|^2\delta(\omega_1 - \omega_k^{xx})\delta(\omega_2 - \omega_l^{xx})$. They depend on the interband exciton, μ_a^x, and the intraband biexciton, μ_{kl}^{xx}, transition dipoles.

The key intensive quantity in Eq. (2) is the effective Coulomb interaction which we define as the rms of the interband Coulomb matrix elements connecting the states with frequencies falling into $[\omega_1, \omega_1 + d\omega_1]$ and $[\omega_2, \omega_2 + d\omega_2]$ intervals,

$$V_{\text{eff}}^{x,xx}(\omega_1,\omega_2) = \left(\frac{V}{v}\right)^2\left[\sum_{a,m}|V_{a,m}^{x,xx}|^2 \frac{\delta(\omega_1 - \omega_a^x)\delta(\omega_2 - \omega_m^{xx})}{\sum_b \delta(\omega_1 - \omega_b^x)\sum_n \delta(\omega_2 - \omega_n^{xx})}\right]^{1/2}. \quad (3)$$

Here, ω_a^x (ω_m^{xx}) is the ath exciton (mth biexciton) state frequency and $V_{a,m}^{x,xx}$ is the Coulomb matrix element between these states. The size scaling of $V_{\text{eff}}^{x,xx}$ in NCs reflects the net result of the Coulomb matrix elements' scaling, relaxation of the momentum conservation constraints, and the appearance of new selection rules associated with the confinement potential symmetry. In Eq. (2), $V_{\text{eff}}^{xx}(\omega)$ denotes effective Coulomb coupling between the ground and biexciton states.

Three terms in the right-hand side of Eq. (2) describe the associated photogeneration pathways [24]: In the first term the optically allowed exciton DOS, $\tilde{\rho}_x(\omega_{pm})$, depends on the pump frequency indicating resonant production of single excitons subsequently scattered to the biexciton states. This is the indirect biexciton photogeneration pathway predicted by IESM [24]. The second term contains biexciton DOS, $\rho_{xx}(\omega_{pm})$, depending on the pump frequency indicating the direct biexciton photogeneration through virtual exciton states. Finally, the last term describes the pathway involving direct biexciton generation by optical stabilization of the scattering processes between the ground state and the biexciton manifold. The last two pathways were first considered in Refs. [5,14], respectively.

The population relaxation dynamics is described by a set of kinetic equations introduced in Ref. [24] and further transformed to the quasicontinuous frequency representation. They contain II and Auger recombination rates

$$k_{\text{II}}(\omega) = \frac{2\pi}{\hbar^2}[V_{\text{eff}}^{x,xx}(\omega)]^2\rho_{xx}(\omega), \quad (4)$$

$$k_{\text{AR}}(\omega) = \frac{2\pi}{\hbar^2}\left(\frac{v}{V}\right)^2[V_{\text{eff}}^{x,xx}(\omega)]^2\rho_x(\omega), \quad (5)$$

respectively, with $V_{\text{eff}}^{x,xx}(\omega) \equiv V_{\text{eff}}^{x,xx}(\omega,\omega)$. According to Eq. (4), the II rate depends on intensive parameters and therefore has finite value in the bulk limit. In contrast, the Auger rate has uncompensated volume prefactor and vanishes as V^{-2} in the bulk limit. The intraband cooling rates in the kinetic equations are calculated using Ohmic spectral density assuming no phonon bottleneck present in NCs. The total QE is evaluated through numerical solution of the kinetic equations with photogenerated populations used as the initial conditions.

To calculate the electron and hole wave functions in spherically symmetric PbSe NCs and bulk, we use the effective mass formalism of Kang and Wise [26]. The exciton and biexciton wave functions are introduced as uncorrelated configurations of the electron and hole wave

functions to evaluate the transition dipoles and the interband Coulomb matrix elements (see supplemental material [27]). The exciton (biexciton) dephasing rate is set to 50 meV (100 meV) which is an order of magnitude consistent with Ref. [20]. To account for degeneracy of the exciton (biexciton) states associated with four equivalent L valleys, the exciton (biexciton) population is multiplied by factor 4 (16). Introducing energy independent effective electron-phonon coupling in the high DOS region, the intraband cooling rates are obtained by fitting the total relaxation time, $\tau_{\rm ph}$, to reproduce the experimentally observed values in the range $0.5 < \tau_{\rm ph} < 5.0$ ps [13,19]. The Monte Carlo sampling is used to handle ensembles of NCs with 5% size distribution.

Figure 1 shows monotonic increase of the calculated photogeneration QE in the NC ensemble to the bulk values as the NC mean diameter increases. To explain this trend, we first look at the contributions of three photogeneration pathways [Eq. (2)] to the biexciton quantum yield, $\eta_{xx} =$ QE $-$ 1. According to the inset of Fig. 1, the contribution of the last pathway [light gray (green) line] is negligible. The other two become equal above the photogeneration energy threshold, $\sim$1.5 eV. Taking into account the resonant nature of the denominator in the first two terms of Eq. (2), the integral convolutions can be calculated. This results in the first and second term identical contributions to η_{xx} as observed in Fig. 1. Hence, the total biexciton population acquires very simple dependence

$$N_{xx}(\omega_{pm}) = k_{\rm II}(\omega_{pm}) N_x(\omega_{pm})/\gamma_{\rm eff}, \qquad (6)$$

on the II rate, $k_{\rm II}$, photogenerated exciton population, N_x, and the effective exciton-biexciton dephasing rate, $\gamma_{\rm eff}$. As a result, the photogeneration QE becomes dependent only on the II rate and effective dephasing rate, QE $=$ $1 + k_{\rm II}/\gamma_{\rm eff}$. To check this relation, we calculated QE using the II rate described by Eq. (4) (Fig. 2) with

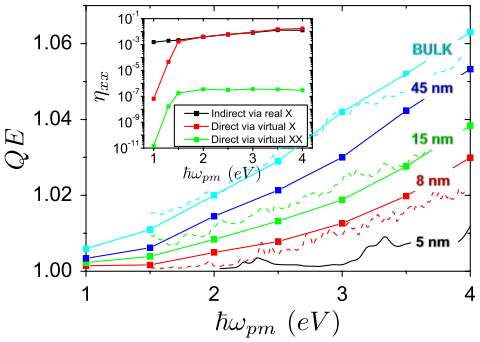

FIG. 1 (color online). Photogeneration QE versus pump energy for PbSe NCs of diameter $d = 5, 8, 15, 45$ nm and bulk. Solid lines mark QE calculated using general expressions for populations from Ref. [24]. Dashed lines show approximate results ($d = 8$, 15 nm NCs and bulk) due to Eq. (6). The inset shows biexciton quantum yield associated with each photogeneration pathway for $d = 15$ nm.

$\hbar\gamma_{\rm eff} = 50$ meV. According to Fig. 1, the latter QE (dashed lines) well reproduces the trends of the "exact" calculations (solid lines).

The analysis above leads to an important conclusion that in the absence of interference destroyed by high DOS and the interband dephasing processes, the photogeneration becomes a resonant process. Furthermore, the biexciton generation described by Eq. (6) can be interpreted as a single II event of the exciton population occurring on the dephasing time scale, $\gamma_{\rm eff}^{-1}$. Previous studies of photogeneration processes [5,14] implicitly assumed constructive interference within the second and the third pathways. The assumption led to significant overestimation of photogeneration QE. Established linear dependence between the photogenerated QE and II rate [Fig. 2(b)] is a key factor in explaining the QE variation with NC size observed in Fig. 1. According to the inset of Fig. 2(a), the effective Coulomb interaction [Eq. (3)] entering II rate [Eq. (4)] is enhanced in NCs compared to the bulk limit just by a factor of 2. In contrast, our calculations show that the biexciton DOS [Fig. 2(a)] reduction in NCs due to quantum confinement fully overplays the effective Coulomb enhancement. The dominant role of the DOS in the II rate leads to the monotonic increase of QE in NC with their size increasing as observed in Fig. 1. This has also been found in Ref. [13].

In contrast to the II rate [Eq. (4)], the volume scaling of the Auger recombination rate [Eq. (5)] makes this competing process negligible as the NC diameter increases. Therefore, the QE associated with the population relaxation is fully determined by the interplay between comparable II and cooling $\tau_{\rm ph}$ times. As a result, the total (i.e., photogeneration and population relaxation) QE has the same trend with the NCs size variation (Fig. 3) as the II rate [Fig. 2(b)] and never exceeds the bulk values. For comparison, the experimental data for PbSe NCs [11] and the bulk [13] are also shown in the plot. Solid lines in Fig. 3 show QE calculated for the intraband cooling time $\tau_{\rm ph} = 1.0$ ps, which provides the best fit for the bulk [13]. Generally, the theory reproduces the experimental trends in bulk (also supporting the adopted model for the phonon assisted cooling). Note that for $\hbar\omega_{\rm ph} \gtrsim 3.6$ eV, where the

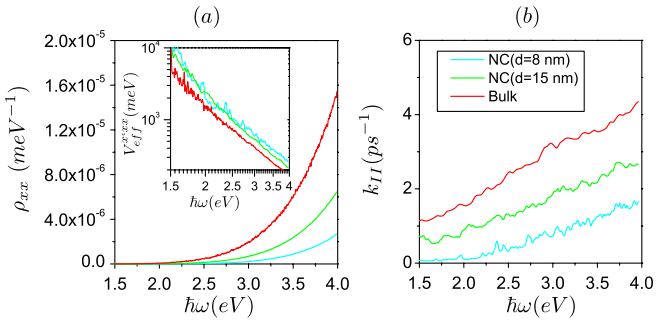

FIG. 2 (color online). Calculated (a) intensive biexciton DOS, (inset) effective Coulomb interaction, and (b) II rate versus energy for PbSe NCs of diameter $d = 8, 15$ nm and bulk.

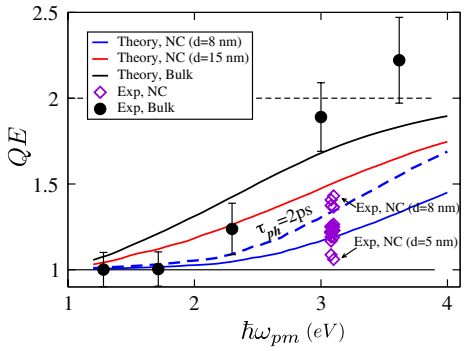

FIG. 3 (color online). Total QE as a function of pump energy calculated for PbSe NCs of diameter $d = 8, 15$ nm and bulk. Solid (dashed) lines present calculations with $\tau_{ph} = 1$ ps ($\tau_{ph} = 2$ ps). For comparison, diamonds and dots mark experimental data from Refs. [11,13], respectively.

triexciton generation appears in experiment (QE > 2 in Fig. 3), the application of our model becomes limited. To get better agreement with experiment for NC of $d = 8$ nm, we had to increase the cooling time up to $\tau_{ph} = 2$ ps (blue dashed line). The increase of τ_{ph} can be attributed to the quantum-confinement-induced increase in the level spacing [28]. The photogeneration contribution (Fig. 1) to the total QE (Fig. 3) is small ($\sim 5\%$). This follows from the fact that the photogeneration is a single II event occurring on a short (< 100 fs) dephasing time scale. In contrast, during the population relaxation multiple II events take place on much longer ($\gtrsim 1$ ps) time scale and provide a major contribution to QE.

To conclude, use of IESM parametrized by the effective mass Hamiltonian allowed us to investigate the mechanisms involved in the photogeneration and population relaxation processes contributing to CM in PbSe NCs and bulk. We argue that direct photogeneration has the impact ionization nature and makes weak contribution to the total QE. The use of intensive DOS and effective Coulomb interaction further allowed for a rigorous analysis of the QE scaling with NC size and comparison with the well-defined bulk limit. We have found that QE in NCs plotted on absolute energy scale does not exceed that in bulk. This is in agreement with reported experimental data and confirms that the quantum-confinement-induced reduction in the biexciton DOS makes a dominant contribution to QE. Finally, note that the power performance of photovoltaic devices depends on the band gap scaling, and even for the case of weak Coulomb enhancement, the NCs are potentially good candidates for such applications. Increase in the effective Coulomb interaction and biexciton DOS through the nanoscale heterostructuring and surface functionalization should further improve their prospective performance.

This work was supported by the BES Office, DOE, Los Alamos LDRD funds, and CNLS. We thank V. Klimov and D. Smith for stimulating discussions and comments on the manuscript.

*apiryat@lanl.gov

[1] S. Kolodinski, J. Werner, T. Wittchen, and H. Queisser, Appl. Phys. Lett. **63**, 2405 (1993).
[2] A. J. Nozik, Physica (Amsterdam) **14E**, 115 (2002).
[3] R. D. Schaller and V. I. Klimov, Phys. Rev. Lett. **92**, 186601 (2004).
[4] R. J. Ellingson *et al.*, Nano Lett. **5**, 865 (2005).
[5] R. D. Schaller, V. M. Agranovich, and V. I. Klimov, Nature Phys. **1**, 189 (2005).
[6] G. Nair and M. G. Bawendi, Phys. Rev. B **76**, 081304(R) (2007).
[7] G. Nair, S. M. Geyer, L.-Y. Chang, and M. G. Bawendi, Phys. Rev. B **78**, 125325 (2008).
[8] M. Ben-Lulu *et al.*, Nano Lett. **8**, 1207 (2008).
[9] J. J. H. Pijpers *et al.*, J. Phys. Chem. C **112**, 4783 (2008).
[10] M. C. Beard *et al.*, Nano Lett. **9**, 836 (2009).
[11] J. A. McGuire *et al.*, Acc. Chem. Res. **41**, 1810 (2008).
[12] J. A. McGuire *et al.*, Nano Lett. **10**, 2049 (2010).
[13] J. J. H. Pijpers *et al.*, Nature Phys. **5**, 811 (2009).
[14] V. I. Rupasov and V. I. Klimov, Phys. Rev. B **76**, 125321 (2007).
[15] A. Shabaev, A. L. Efros, and A. J. Nozik, Nano Lett. **6**, 2856 (2006).
[16] W. M. Witzel, A. Shabaev, C. S. Hellberg, V. L. Jacobs, and A. L. Efros, Phys. Rev. Lett. **105**, 137401 (2010).
[17] A. Franceschetti, J. M. An, and A. Zunger, Nano Lett. **6**, 2191 (2006).
[18] E. Rabani and R. Baer, Nano Lett. **8**, 4488 (2008).
[19] G. Allan and C. Delerue, Phys. Rev. B **77**, 125340 (2008).
[20] O. V. Prezhdo, Acc. Chem. Res. **42**, 2005 (2009).
[21] E. Rabani and R. Baer, Chem. Phys. Lett. **496**, 227 (2010).
[22] C. Delerue, G. Allan, J. J. H. Pijpers, and M. Bonn, Phys. Rev. B **81**, 125306 (2010).
[23] L. Silvestri and V. M. Agranovich, Phys. Rev. B **81**, 205302 (2010).
[24] A. Piryatinski and K. A. Velizhanin, J. Chem. Phys. **133**, 084508 (2010).
[25] M. C. Beard *et al.*, Nano Lett. **10**, 3019 (2010).
[26] I. Kang and F. W. Wise, J. Opt. Soc. Am. B **14**, 1632 (1997).
[27] See supplemental material at http://link.aps.org/supplemental/10.1103/PhysRevLett.106.207401 for parametrization of exciton and biexciton states, dipole moments, and Coulomb matrix elements.
[28] C. Bonati *et al.*, Phys. Rev. B **76**, 033304 (2007).